



Molecular structure and sour gas surface chemistry of supported K_2O/WO_3 / Al_2O_3 catalysts

Minghui Zhu^a, Bin Li^a, Jih-Mirn Jehng^a, Lohit Sharma^a, Julian Taborda^a, Lihua Zhang^b, Eric Stach^{b,c}, Israel E. Wachs^a, Zili Wu^{d,e}, Jonas Baltrusaitis^{a,*}

^a Department of Chemical and Biomolecular Engineering, Lehigh University, B336 Iacocca Hall, 111 Research Drive, Bethlehem, PA 18015, USA

^b Brookhaven National Laboratory, Center for Functional Nanomaterials, Upton, NY 11973, USA

^c Materials Science and Engineering, University of Pennsylvania, Philadelphia, PA 19104, USA

^d Chemical Sciences Division, Oak Ridge National Laboratory, Oak Ridge, TN, 37831, USA

^e Center for Nanophase Material Science, Oak Ridge National Laboratory, Oak Ridge, TN, 37831, USA



ARTICLE INFO

Keywords:

$K_2O/WO_3/Al_2O_3$
Catalyst
in situ
 CO_2
 SO_2

ABSTRACT

Molecular structures of the unpromoted and K_2O -promoted supported WO_3/Al_2O_3 catalysts were studied with *in situ* Raman and UV-vis spectroscopy. *In situ* Raman spectra revealed that supported 20% WO_3/Al_2O_3 corresponds to near monolayer coverage of isolated and oligomeric surface WO_x species on Al_2O_3 . Above monolayer surface WO_x coverage (21% WO_3/Al_2O_3), crystalline WO_3 nanoparticles are also present. The addition of K_2O to the supported WO_3/Al_2O_3 catalyst increased the concentration of isolated surface WO_x species and did not form K_2WO_4 nanoparticles. The reducibility of the tungsten oxide structures depends on their structures (2D or 3D) and the K_2O promoter. Their interaction with acidic CO_2 and SO_2 gases was also investigated. Adsorption of CO_2 creates several surface carbonate species of varying acidity that were detected using a combination of *in situ* IR and mass spectroscopy. Adsorbed bicarbonate form on weakly basic surface sites on tungsten oxide monolayer WO_3/Al_2O_3 catalyst as well as in the presence of low 2.5% K_2O loading. At high 5% K_2O loading, the presence of the strong surface basic sites yields adsorbed carbonates. After SO_2 pretreatment, however, new strongly adsorbed sulfate appears on the surface that inhibits CO_2 adsorption.

1. Introduction

Abundant, yet difficult to utilize *sour* natural gas contains a large number of acidic components such as CO_2 and H_2S at quite high concentrations. Approximately 40% of the world's conventional natural gas reserves contain significant amounts of H_2S and CO_2 while about 30% contain < 15% CO_2 and 1–15% H_2S [1]. These sour gas concentrations are treatable with conventional methods such as amine absorption/desorption [2–4], but the question remains whether this can be achieved economically. A major problem of conventional sour gas removal from natural gas remains utilization of the large amounts of environmentally non-friendly CO_2 and H_2S byproducts. Conventionally, the acidic CO_2 is emitted into the atmosphere acting as a major greenhouse gas motivating the need for new catalytic methods of converting CO_2 into hydrocarbons [5–7]. The H_2S , however, is a sour gas with high toxicity that is oxidized via the Claus process to yield unreactive elemental sulfur that can be used for the manufacture of sulfuric acid or deposited in chemical landfills [8]. An alternative is to directly convert H_2S and carbon oxides with the addition of H_2 to form

the reactive CH_3SH intermediate that can be further converted to a mixture of paraffin and olefins to avoid the high conventional CH_4 - CO_2 - H_2S separation costs [9–16]. Early studies have revealed the catalytic activity of supported tungsten based catalysts for such reaction, as well as the promotional effect of K_2O [17–20]. For example, Barrault et al. have achieved high selectivity towards two major products of CO (49%) and CH_3SH (51%) from a mixture of CO_2 , H_2S and H_2 by using a supported 10% $K_2WO_4/\gamma-Al_2O_3$ catalyst [20].

As a widely used catalyst, supported WO_3/Al_2O_3 is active for a variety of reactions such as alkane metathesis [21,22], hydrogenation [23,24], dehydration [25,26], hydro-desulfurization [27,28] and hydrocarbon cracking [29,30]. Its molecular structure and surface chemistry have been extensively investigated in the literature, showing the existence of isolated, oligomeric and crystallized WO_x species depending on catalyst loadings [31–33]. Addition of K_2O has been found to play an important role as a promoter for the supported WO_3/Al_2O_3 catalyst and favors the production of methyl mercaptan from methanol and hydrogen sulfide [34]. Much less research, however, has been dedicated to elucidating the structure of the K_2O -promoted supported

* Corresponding author.

E-mail address: job314@lehigh.edu (J. Baltrusaitis).

WO_x/Al₂O₃ catalyst

In this work, we aim at elucidating the promotional effect of K₂O to WO₃/Al₂O₃ catalyst with an emphasis on its modification of surface chemistry, especially the interplay with two weakly adsorbed reactant molecules including H₂ and CO₂. In addition, the performance of competitive CO₂ adsorption under sulfur containing acidic environment was evaluated with the aid of SO₂ pre-adsorption. The application of modern characterization techniques including STEM, *in situ* Raman, *in situ* UV-vis, *in-situ* Diffuse Reflectance Infrared Fourier Transform Spectroscopy (DRIFTS), H₂ temperature programmed reduction (TPR) and CO₂ temperature programmed desorption (TPD) has enabled the understanding of the surface chemistry for K₂O promoted WO_x/Al₂O₃ catalyst. Those fundamental insights will have the potential to guide the rational design of improved tungsten based catalysts for direct methyl mercaptan synthesis from sour natural gas.

2. Experimental

2.1. Catalyst preparation

Ternary K₂O promoted WO₃/Al₂O₃ catalysts (K₂O/WO₃/Al₂O₃) were synthesized with incipient-wetness impregnation method using water soluble ammonium metatungstate ((NH₄)₆H₂W₁₂O₄₀·xH₂O) and potassium hydroxide (KOH) as precursors [35,36]. The active catalyst support was Toyota γ-Al₂O₃ with surface area 170 m²/g. The synthesis involved two separate steps. In particular, tungsten oxide was initially impregnated into the γ-Al₂O₃ support and followed by impregnation of K₂O in the second step. Specific amount of ammonium metatungstate ((NH₄)₆H₂W₁₂O₄₀·xH₂O) was placed into a ceramic crucible, dissolved in 1 ml of deionized water and 1 gram of γ-Al₂O₃ was added into the ceramic crucible and stirred for 30 min. The samples were dried under ambient conditions overnight, further dried at 120 °C for 16 h and finally calcined at 500 °C for 4 h.

2.2. Scanning transmission electron microscopy

The morphology of the catalyst particles was investigated using a dedicated Scanning Transmission Electron Microscope (STEM) (Hitachi 2700 C) operating at 200 kV.

2.3. *In situ* UV-vis diffuse reflectance spectroscopy (DRS)

In situ UV-vis DR spectra of WO₃/Al₂O₃ and K₂O/WO₃/Al₂O₃ catalysts were obtained using a Cary 5000 UV-vis NIR spectrometer. The samples were loaded into an *in situ* cell (Harrick, HVC-DR2) and dehydrated under the flow of 10% O₂/He at 400 °C for 1 h. A magnesium oxide sample was used as the reflectance standard for collecting baseline in the 200–800 nm region.

2.4. *In situ* Raman spectroscopy

Raman spectra were collected using a LabRam-HR spectrometer (Horiba-Jobin Yvon) equipped with a confocal microscope, 2400/900 grooves/mm gratings and a notch filter. The 532-nm visible laser was focused on the samples using a confocal microscope equipped with a 50× long working distance objective (Olympus, BX-30- LWD). The scattered photons were directed and focused onto a single-stage monochromator and measured with a UV-sensitive LN₂-cooled CCD detector (Horiba, CCD-3000V). Catalyst samples were placed in an environmentally controlled high-temperature cell reactor (Harrick). Dehydrated spectra were collected after catalysts were dehydrated in the stream of 10% O₂/Ar at 400 °C for 1 h.

2.5. H₂-temperature programmed reduction (TPR) spectroscopy

The H₂-TPR experiments were carried out using an Altamira

Instruments (AMI-200) connected to a TCD detector. Approximately 30 mg of catalyst was loaded into a U-tube sample holder for analysis. The catalysts tested were first dehydrated under 10% O₂/Ar at 400 °C for 1 h then cooled down to 100 °C. The H₂-TPR experiments were then performed by ramping up the temperature under 10% H₂/Ar (30 ml/min) at a rate of 10 °C/min.

2.6. CO₂-temperature programmed desorption (TPD) spectroscopy

The CO₂-TPD experiments were performed using an Altamira Instruments system (AMI-200) with a TCD detector. Approximately 50 mg of catalyst was loaded into a U-tube sample holder for analysis. The catalysts tested were first dehydrated under 10% O₂/Ar at 400 °C for 1 h then cooled down to room temperature. The catalysts were then saturated under CO₂ flow for 1 h and flushed with He for 30 min. After the He flush, the CO₂-TPD experiments were performed by ramping the temperature under He at a rate of 10 °C/min.

2.7. Surface chemistry and acidity

Catalyst surface acidity was examined using a combination of NH₃ probe molecule and infrared spectroscopy. A Thermo Nicolet iS50 infrared spectrometer equipped with a Mercury-Cadmium-Tellurium (MCT) liquid nitrogen cooled detector was used with a Harrick Praying Mantis™ diffuse reflection accessory and ZnSe windows for determination of the acid sites. Catalysts were initially dehydrated by heating to 400 °C (heating rate of 10 °C/min) and holding at 400 °C for 1 h under air flow (30 mL/min). The *in situ* IR spectra were collected under N₂ (30 mL/min) while cooling down at 400 °C, 300 °C, 200 °C and 120 °C. Subsequently, N₂ was replaced with a flow of 1% NH₃/N₂ (30 mL/min; 30 min). Physisorbed NH₃ was removed by flowing N₂ (30 mL/min; 30 min). Spectra were then continuously recorded every minute during the temperature programming until 400 °C under 30 mL/min N₂ flow. The spectra of dehydrated catalysts at specified temperatures were subtracted from the spectra containing contributions of the catalyst and adsorbed NH₃ surface species at the same temperature.

2.8. *In situ* diffuse reflectance infrared fourier transformed spectroscopy (DRIFTS)

DRIFTS experiments were performed using diffuse reflectance mode in a Thermo Nicolet Nexus 670 spectrometer. Quadrupole mass spectrometer (Omnistar GSD-301 O₂, Pfeiffer Vacuum) was used to analyze the reaction products from the DRIFTS cell (Pike Technologies HC-900). Catalyst samples were first dehydrated under 5%O₂/He at 500 °C for 1 h and then cooled down to room temperature. After that, 30 mL/min CO₂ (2% CO₂/N₂) was introduced for 30 min, followed by a 20-min flush with He. The samples were then heated up to 500 °C under He with a rate of 10 °C/min. The catalysts then were cooled down to room temperature again, pre-treated with 30 mL/min SO₂ (210 ppm) for 30 min and flushed with He for 20 min. The pretreated samples were further saturated with CO₂ by flowing 30 mL/min 2% CO₂/N₂ for 30 min and flushed with He for 20 min and subsequently heated up under flowing He to 500 °C with a rate of 10 °C/min.

3. Results and discussion

3.1. Surface structure

The detailed composition, K/W atomic ratio and BET surface areas of all prepared catalysts were shown in Table 1. The Eg values were also calculated and provided from the corresponding *in-situ* UV-vis spectra under dehydrated conditions (Fig. 1). Those values are within the range of oligomers of WO₆ (2.8 eV) and isolated WO₄ units (5.2 eV), indicating the coexistence of isolated and oligomeric species [37]. The smaller Eg value for 20% WO₃/Al₂O₃ than 21% WO₃/Al₂O₃ reflects the

Table 1

Composition, K/W atomic ratio, BET surface area and *in situ* UV-vis DRS Eg values for dehydrated supported $\text{WO}_3/\text{Al}_2\text{O}_3$ and $\text{K}_2\text{O}/\text{WO}_3/\text{Al}_2\text{O}_3$ catalysts.

Sample	K/W atomic ratio	BET (m^2/g)	Eg (eV)
Al_2O_3	–	133	–
21% $\text{WO}_3/\text{Al}_2\text{O}_3$	–	99	4.1
20% $\text{WO}_3/\text{Al}_2\text{O}_3$	–	105	4.5
2.5% $\text{K}_2\text{O}/19\% \text{WO}_3/\text{Al}_2\text{O}_3$	0.65	113	4.5
5% $\text{K}_2\text{O}/19.5\% \text{WO}_3/\text{Al}_2\text{O}_3$	1.26	95	4.9

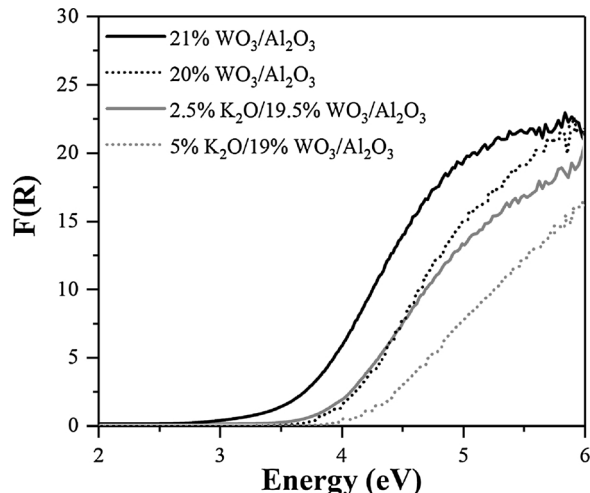


Fig. 1. *In situ* UV-vis spectra of dehydrated 20% $\text{WO}_3/\text{Al}_2\text{O}_3$, 21% $\text{WO}_3/\text{Al}_2\text{O}_3$, 2.5% $\text{K}_2\text{O}/19.5\% \text{WO}_3/\text{Al}_2\text{O}_3$ and 5% $\text{K}_2\text{O}/19\% \text{WO}_3/\text{Al}_2\text{O}_3$ catalysts.

presence of a greater amount of oligomeric tungsten oxide component in the latter catalyst. Adding small amount of potassium oxide ($\text{K}/\text{W} = 0.65$) has negligible effect on UV-vis Eg value as well as the relative populations of isolated and oligomeric surface WO_x species. The addition of more potassium oxide ($\text{K}/\text{W} = 1.26$), however, increases the UV-vis Eg value to 4.9 eV, reflecting an increase in the population of isolated surface WO_x species at the expense of the oligomeric surface WO_x species.

Catalyst surface information and the interaction between K and W species were further studied with *in situ* Raman. Crystalline WO_3 exhibits strong and sharp Raman bands at 273, 719 and 809 cm^{-1} , while crystalline K_2WO_4 possesses strong and sharp Raman bands at 324 and 927 cm^{-1} , reflecting the presence of oligomeric WO_6 and isolated WO_4 sites in the WO_3 and K_2WO_4 crystals, respectively [37]. The Raman spectrum of supported 20% $\text{WO}_3/\text{Al}_2\text{O}_3$ exclusively exhibits a band at 1021 cm^{-1} and is assigned to surface WO_x species on the Al_2O_3 support, which is also confirmed by STEM image (Figs. 2b, S1). The Raman band at 1021 cm^{-1} corresponds to the stretching mode of isolated and oligomeric mono-oxo $\text{O}=\text{WO}_{4/5}$ surface species [32]. Supported 21% $\text{WO}_3/\text{Al}_2\text{O}_3$ catalyst contains the surface $\text{O}=\text{WO}_{4/5}$ species (1021 cm^{-1}) and crystalline WO_3 nanoparticles (NPs) with strong characteristic bands at 260, 327, 711 and 804 cm^{-1} . The much stronger intensity for crystalline nanoparticles is due to the higher Raman cross sections. The Raman spectra for the K-promoted 2.5% $\text{K}_2\text{O}/19.5\% \text{WO}_3/\text{Al}_2\text{O}_3$ and 5% $\text{K}_2\text{O}/19\% \text{WO}_3/\text{Al}_2\text{O}_3$ catalysts exhibit the $\text{W}=\text{O}$ bands at 985 cm^{-1} and 963 cm^{-1} with the absence of crystalline K_2WO_4 bands [38]. The shift of the $\text{W}=\text{O}$ Raman band from 1021 to $963\text{--}985\text{ cm}^{-1}$ indicates that the potassium is interacting with the surface WO_x species and reflects lengthening of the $\text{W}=\text{O}$ bond [33].

3.2. H_2 -TPR

The interaction of the supported 20% $\text{WO}_3/\text{Al}_2\text{O}_3$, 21% $\text{WO}_3/\text{Al}_2\text{O}_3$, 2.5% $\text{K}_2\text{O}/19.5\% \text{WO}_3/\text{Al}_2\text{O}_3$ and 5% $\text{K}_2\text{O}/19\% \text{WO}_3/\text{Al}_2\text{O}_3$ catalysts

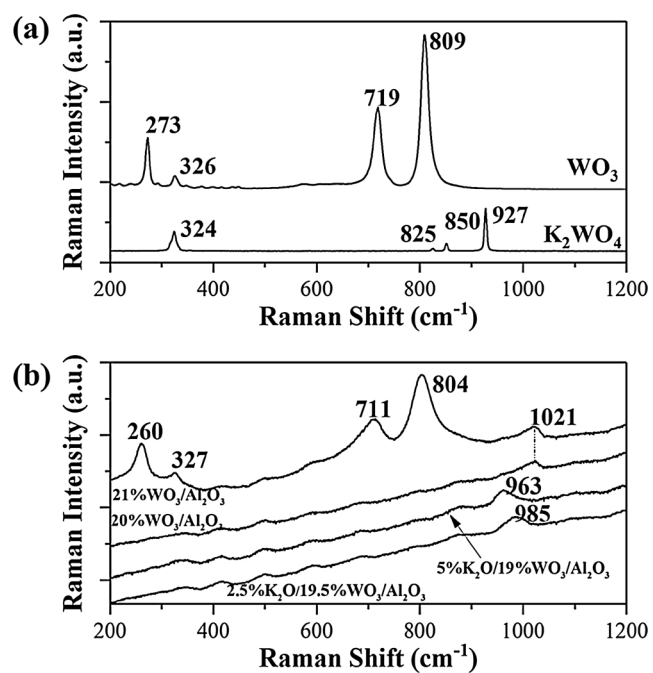


Fig. 2. (a) Raman spectra of crystalline WO_3 and K_2WO_4 . (b) *In situ* Raman spectra of dehydrated 20% $\text{WO}_3/\text{Al}_2\text{O}_3$, 21% $\text{WO}_3/\text{Al}_2\text{O}_3$, 2.5% $\text{K}_2\text{O}/19.5\% \text{WO}_3/\text{Al}_2\text{O}_3$ and 5% $\text{K}_2\text{O}/19\% \text{WO}_3/\text{Al}_2\text{O}_3$ catalysts.

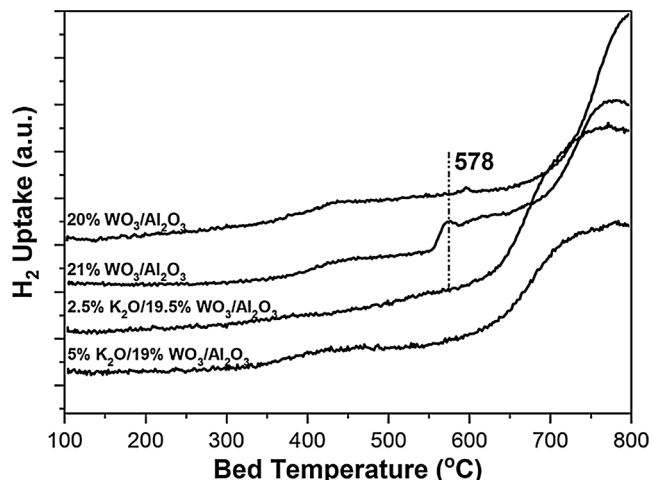


Fig. 3. H_2 -TPR spectra of supported 20% $\text{WO}_3/\text{Al}_2\text{O}_3$, 21% $\text{WO}_3/\text{Al}_2\text{O}_3$, 2.5% $\text{K}_2\text{O}/19.5\% \text{WO}_3/\text{Al}_2\text{O}_3$ and 5% $\text{K}_2\text{O}/19\% \text{WO}_3/\text{Al}_2\text{O}_3$ catalysts.

with H_2 molecules was assessed with H_2 -TPR and the results are shown in Fig. 3. All four catalysts exhibited reduction peak at a temperature higher than 600 °C , corresponding to the reduction of surface tungsten oxide species. Such a high reduction temperature has also been previously confirmed both theoretically and experimentally [39,40]. The supported 21% $\text{WO}_3/\text{Al}_2\text{O}_3$ catalyst possesses an extra reduction peak at 578 °C that is assigned to the reduction of crystalline WO_3 NPs [41,42]. Addition of K_2O to the catalyst shifted the reduction peak of surface tungsten species to lower temperature ($T_p \sim 725\text{ °C}$) and is probably due to enhanced H_2 adsorption or dissociation on K atoms.

3.3. CO_2 -TPD

The desorption of CO_2 , SO_2 and H_2O from dehydrated catalysts, with and without SO_2 pretreatment, during temperature programming are shown in Fig. 4 (a–d). In the absence of SO_2 pretreatment, the supported 20% $\text{WO}_3/\text{Al}_2\text{O}_3$ and 21% $\text{WO}_3/\text{Al}_2\text{O}_3$ catalysts exhibit poor

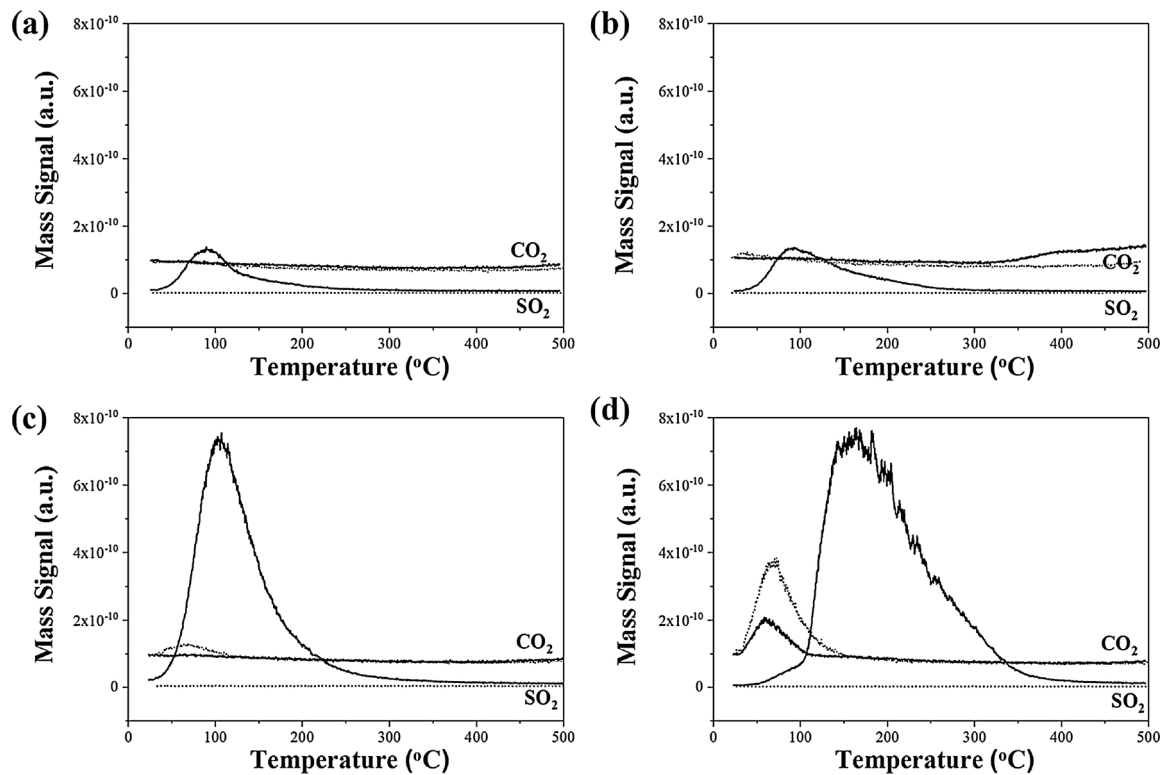


Fig. 4. (a–d) Mass spec signal of CO₂ and SO₂ obtained during CO₂-TPD of catalysts with and without SO₂ pretreatment. (a) 21% WO₃/Al₂O₃, (b) 20% WO₃/Al₂O₃, (c) 2.5% K₂O/19.5% WO₃/Al₂O₃, (d) 5% K₂O/19% WO₃/Al₂O₃. The solid lines represent the sample with SO₂ pretreatment and the dot lines represent the sample without SO₂ pretreatment.

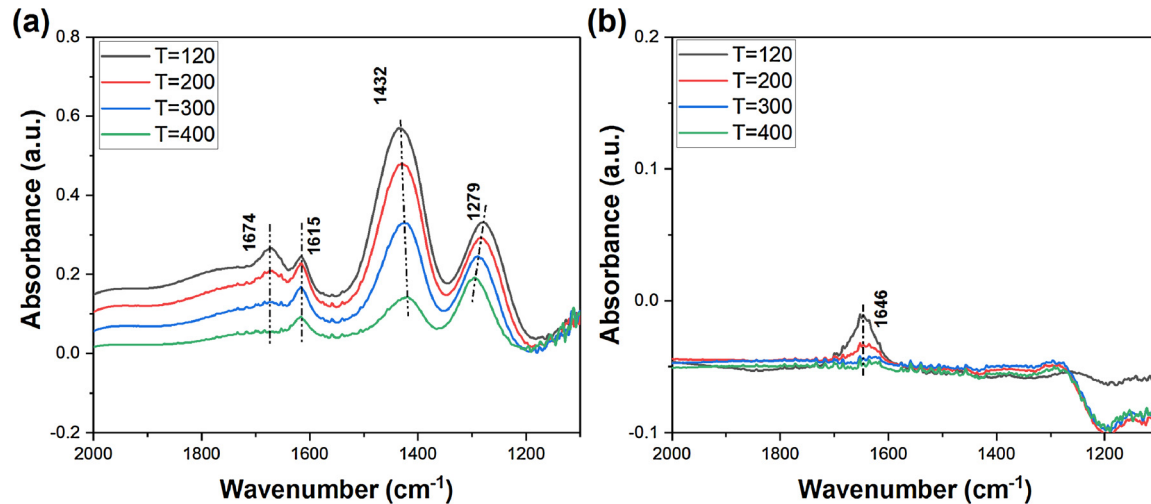


Fig. 5. NH₃-IR spectra obtained from (a) 20% WO₃/Al₂O₃, (b) 5% K₂O/19% WO₃/Al₂O₃.

CO₂ adsorption capacity with barely a trace of CO₂ desorption at ~50 °C (see Fig. 4 (a and d)) because acidic CO₂ very weakly interacts with the acidic surface WO_x sites [43]. The absence of CO₂ adsorption capacity of these two supported WO₃/Al₂O₃ catalysts reflects the presence of a surface WO_x monolayer that covers the basic sites of the alumina support. The addition of potassium oxide enhances CO₂ adsorption as reflected by CO₂ desorption at ~50 °C because of the interaction of acidic CO₂ with basic surface K₂O sites. The CO₂ adsorption capacity of the dehydrated catalysts follows the order 5% K₂O/19% WO₃/Al₂O₃ > 2.5% K₂O/19.5% WO₃/Al₂O₃ > 20% WO₃/Al₂O₃ > 21% WO₃/Al₂O₃.

The adsorption capacity of SO₂ on the catalysts is shown in Fig. 4 and is significantly greater than that of CO₂ because of the stronger acidity of SO₂ compared to CO₂. Unlike the very weak CO₂ adsorption

on the K-free supported WO₃/Al₂O₃ catalysts, SO₂ modestly adsorbs on the K-free supported WO₃/Al₂O₃ catalysts. The adsorption capacity of SO₂ greatly increases, by ~5×, with K₂O content because of the increased number of surface basic sites introduced by potassium oxide.

Although there is no H₂O desorption for the catalysts not pretreated with SO₂, as expected for the dehydrated catalysts, all the supported WO₃/Al₂O₃ catalysts exhibit H₂O desorption after SO₂ pretreatment (Fig. S2). The amount of H₂O desorbed appears to decrease with potassium oxide promotion. The formation of H₂O after SO₂ treatment suggests that SO₂ is either reacting with alumina surface hydroxyls or making the catalyst hygroscopic and retains the trace moisture in the environmental cell.

The weak CO₂ adsorption capability was further decreased from the catalysts, especially the K-promoted catalysts, when SO₂ was pre-

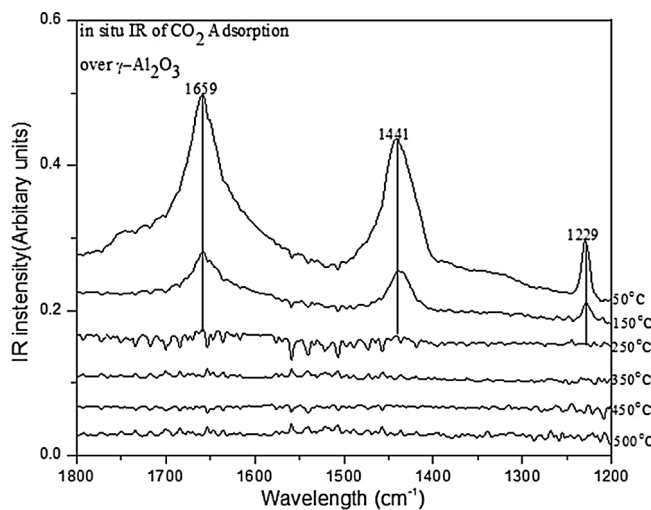


Fig. 6. IR spectra of γ -Al₂O₃ obtained at different temperature after CO₂ adsorption.

adsorbed on the catalysts. The supported 2.5% K₂O/19.5% WO₃/Al₂O₃ catalyst exhibited negligible CO₂ desorption indicating that acidic SO₂ coordinated to the basic surface K₂O sites and blocked coordinating of acidic CO₂. The supported 5% K₂O/19% WO₃/Al₂O₃ catalyst however, still possesses CO₂ adsorption capacity after SO₂ pretreatment reflecting the presence of residual basic surface sites (~50%). The SO₂ pretreatment also appears to slightly weaken the CO₂ binding to the catalyst with T_p decreasing from ~75 to ~60 °C when the supported 5% K₂O/19% WO₃/Al₂O₃ catalyst was exposed to SO₂.

3.4. Surface acidity probed with NH₃ adsorption

The surface acidity of the dehydrated supported WO_x catalysts was probed with NH₃-DRIFTS and the temperature dependent spectrum are presented in Fig. 5. After NH₃ adsorption at 120 °C, the 20% WO₃/Al₂O₃ catalyst (Fig. 5(a)) exhibits IR bands for both adsorbed NH₃ species (1615 and 1279 cm⁻¹) and NH₄⁺ species (1674 and 1432 cm⁻¹) [44,45]. The existence of two type of adsorbed ammonia species clearly demonstrates that surface of the 20% WO₃/Al₂O₃ catalyst possesses both Lewis (NH₃) and Brønsted (NH₄⁺) acidity. Upon increasing the temperature, the population of the adsorbed NH₃ species decrease slower than surface NH₄⁺ species that shows their greater stability on the surface. The NH₃-IR spectrum for the supported 5% K₂O/19% WO₃/Al₂O₃ catalyst is shown in Fig. 5(b) and the addition of potassium greatly modifies the surface acidity of supported WO_x catalyst. The lack of the predominant 1279 cm⁻¹ band for adsorbed NH₃ species and the 1432 cm⁻¹ band for adsorbed NH₄⁺ species suggest that K₂O completely suppressed both Brønsted and Lewis acidity from the surface WO_x species or exposed Al₂O₃ sites. The weak IR band at 1646 cm⁻¹, which diminishes at higher temperature, may arise from adsorbed ammonia species on K sites. Similarly, a sole band at 1610 cm⁻¹ was observed for very low NH₃ coverages on Fe{111} pre-covered with 0.25 monolayer of K and was attributed to antisymmetric deformation mode of ammonia, δ_a [46]. This vibration was attributed specifically to the interaction between ammonia and potassium atoms.

3.5. In-situ DRIFTS using CO₂ and SO₂ as acidic probe molecules

Carbonate in its free ion form has a Raman active vibration of 1063 cm⁻¹ due to the symmetric C–O stretching (ν_1), an IR active

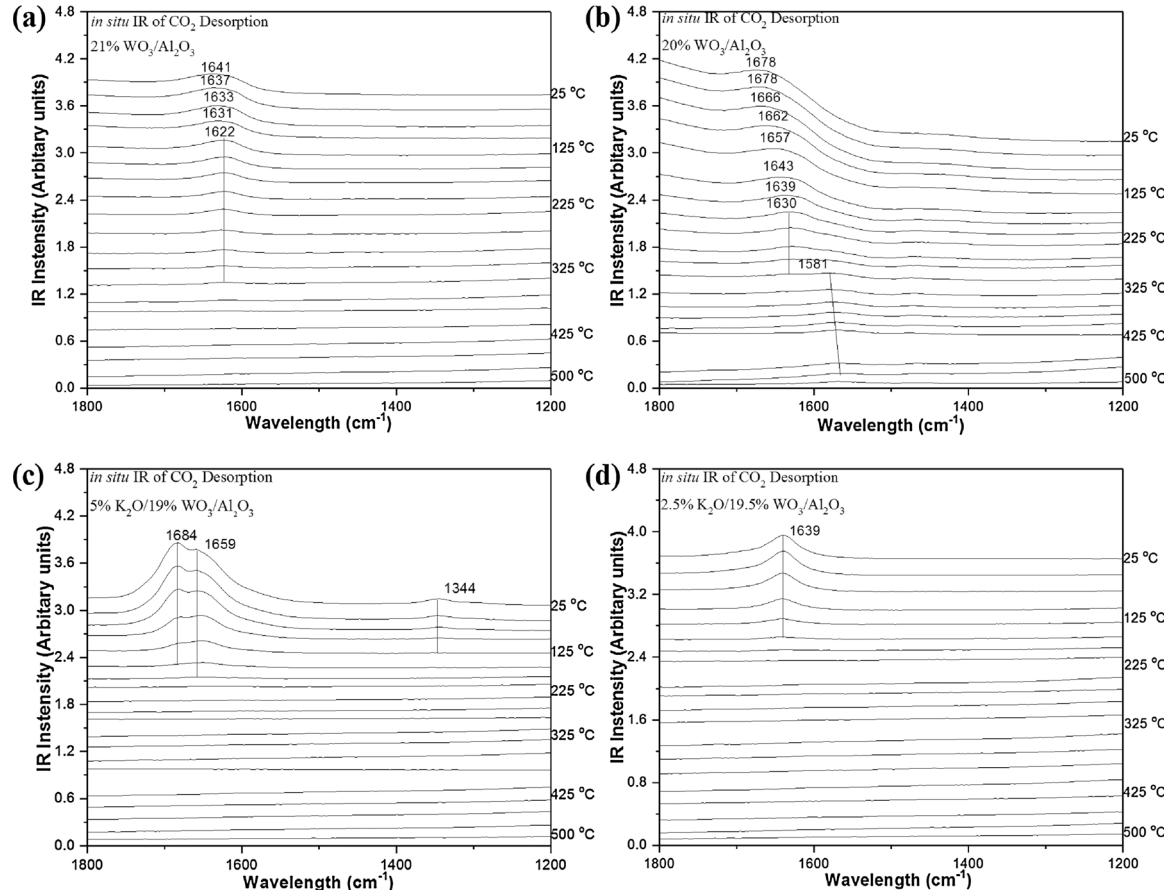


Fig. 7. (a-d) TP-IR spectra of CO₂ adsorption without SO₂ pretreatment obtained at different temperature. (a) 21% WO₃/Al₂O₃, (b) 20% WO₃/Al₂O₃, (c) 5% K₂O/19% WO₃/Al₂O₃ catalysts and (d) 2.5% K₂O/19.5% WO₃/Al₂O₃.

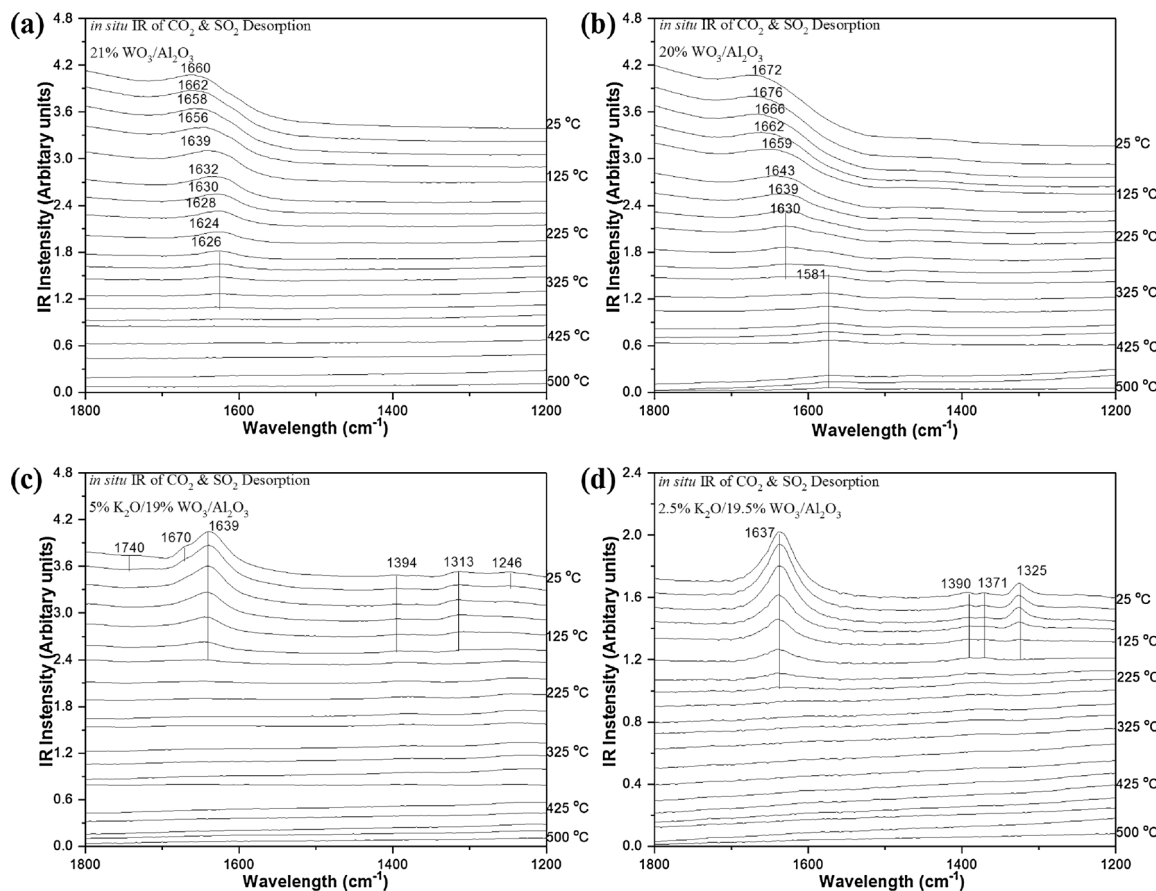


Fig. 8. (a–d) TP-IR spectra of CO_2 adsorption with SO_2 pretreatment obtained at different temperature. (a) 21% $\text{WO}_3/\text{Al}_2\text{O}_3$, (b) 20% $\text{WO}_3/\text{Al}_2\text{O}_3$, (c) 5% $\text{K}_2\text{O}/19\%$ $\text{WO}_3/\text{Al}_2\text{O}_3$ and (d) 2.5% $\text{K}_2\text{O}/19.5\%$ $\text{WO}_3/\text{Al}_2\text{O}_3$.

Table 2
Summary of surface CO_2 and SO_2 adsorption products on $\text{K}_2\text{O}/\text{WO}_3/\text{Al}_2\text{O}_3$ catalysts.

Condition	Samples	Wavelength (cm^{-1})			
Without SO_2 pretreatment	21% $\text{WO}_3/\text{Al}_2\text{O}_3$	1641			
	Assignment	Bidentate-II	Bicarbonate		
	20% $\text{WO}_3/\text{Al}_2\text{O}_3$	1678			
	Assignment	Bidentate-II	Polydentate-I	Bicarbonate	
	5% $\text{K}_2\text{O}/19\%$ $\text{WO}_3/\text{Al}_2\text{O}_3$	1684	1659	1344	
	Assignment	Bidentate-I	Bicarbonate	Monodentate	
With SO_2 pretreatment	2.5% $\text{K}_2\text{O}/19.5\%$ $\text{WO}_3/\text{Al}_2\text{O}_3$	1639			
	Assignment	Bicarbonate			
	21% $\text{WO}_3/\text{Al}_2\text{O}_3$	1660			
	Assignment	Bidentate-II	Bicarbonate		
	20% $\text{WO}_3/\text{Al}_2\text{O}_3$	1672			
	Assignment	Bidentate	Polydentate-I	Bicarbonate	
	5% $\text{K}_2\text{O}/19\%$ $\text{WO}_3/\text{Al}_2\text{O}_3$	1740	1670	1639	1394
	Assignment	Bridged	Bridged	Bidentate-I	$\text{Al}_2(\text{SO}_4)_3$
	2.5% $\text{K}_2\text{O}/19.5\%$ $\text{WO}_3/\text{Al}_2\text{O}_3$	1637	1390	1371	1313
	Assignment	Bidentate-II	$\text{Al}_2(\text{SO}_4)_3$	1325	1246
				Physisorbed SO_2	Asymmetric O-C-O
					Physisorbed SO_2

vibration of 879 cm^{-1} due to out-of-plane deformation (ν_2), and two Raman-IR active vibrations of 1415 and 680 cm^{-1} , due to CO asymmetric stretching (ν_3) and in-plane deformation (ν_4), respectively [47,48]. Changes in molecular symmetry from electrostatic, hydrogen and covalent binding induce important shifts as well as the doubly degenerate ν_3 and ν_4 split. The magnitude of this ν_3 shift is attributed to different binding modes of the carbonate species formed. The surface species and their thermal stability on supported $\gamma\text{-Al}_2\text{O}_3$ after CO_2 adsorption has previously been well investigated in the literature [35,47]. Four types of surface chemisorbed carbonate species were identified: a) monodentate, 2) bidentate (1730–1660 and 1270–1230 cm^{-1}), 3)

bridged surface carbonate (~ 1900 – 1750 cm^{-1} and 1180 cm^{-1}) and 4) bicarbonate (~ 3610 – 3605 , 1650 – 1639 , 1490 – 1440 and 1236 – 1225 cm^{-1}). The temperature-dependent *in situ* IR spectra of $\gamma\text{-Al}_2\text{O}_3$ obtained after CO_2 adsorption are presented in Fig. 6. Adsorption of CO_2 on $\gamma\text{-Al}_2\text{O}_3$ exhibits three peaks (1659 , 1441 and 1229 cm^{-1}) that are attributed to surface bicarbonate species [47]. These are weakly bound to the alumina surface and completely desorb at 250 °C .

The temperature programmed-IR spectra of CO_2 adsorbed 20 and 21% $\text{WO}_3/\text{Al}_2\text{O}_3$ catalysts are shown in Fig. 7a and b, respectively. The 21% $\text{WO}_3/\text{Al}_2\text{O}_3$ catalyst (Fig. 7a) possesses a characteristic band at 1641 cm^{-1} shifts to 1622 cm^{-1} , with increasing temperature and starts to

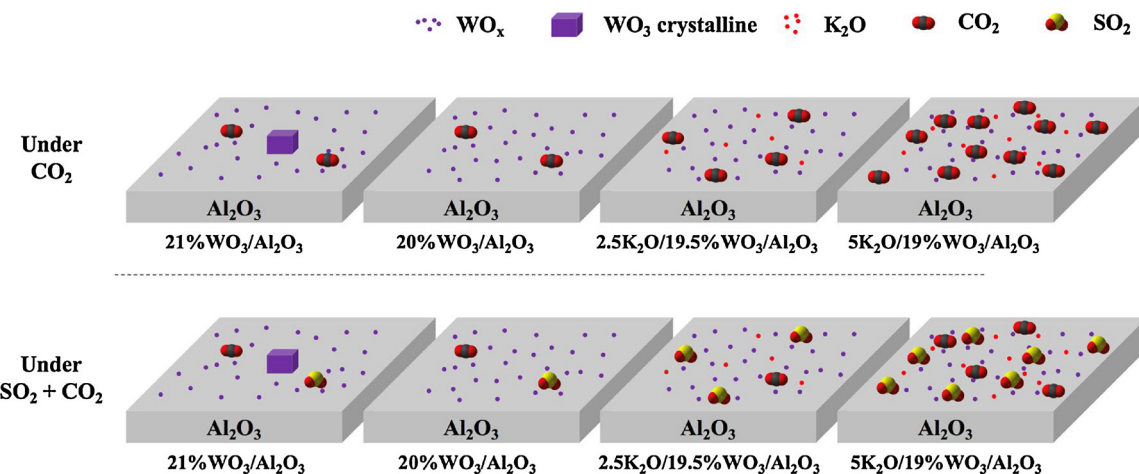


Fig. 9. Pictorial representation of the acid gas, CO_2 and SO_2 , interactions with $\text{WO}_3/\text{Al}_2\text{O}_3$ and $\text{K}_2\text{O}/\text{WO}_3/\text{Al}_2\text{O}_3$ catalyst surfaces.

desorb at 255 °C. The band position and desorbing temperatures (T_d) indicate the presence of bicarbonate species. Alternatively, this shift with temperature can be associated with transformation of adsorbed bicarbonate into more stable bidentate-II carbonate species. This is consistent with the release of gaseous H_2O observed in Fig. 4 where reactive surface hydroxyl recombine and desorb while adsorbed carbonate species are formed. The supported 20% $\text{WO}_3/\text{Al}_2\text{O}_3$ catalyst (Fig. 7b) contains an IR band at 1678 that shifts to 1630 cm^{-1} at 225 °C. That band further transforms into a distinct high temperature-stable carbonate species at 325 °C. According to Figs. 2b and 3, both the supported 20 and 21% $\text{WO}_3/\text{Al}_2\text{O}_3$ catalysts possess a distinct WO_3 surface structure. It can be suggested that when WO_3 nanoparticles are absent on the surface WO_x monolayer the adsorbed CO_2 forms an adsorbed carbonate species at 1581 cm^{-1} . Strong CO_2 interactions with WO_3 nanoparticles, however, are not observed. A detailed literature review based on well-defined organometallic CO_2 -containing molecular infrared vibrations revealed that formate species can form with recorded vibration at 1612 cm^{-1} [47,49]. Other adsorbed CO_2 species on the W binding centers, such as $\mu_2\text{-}\eta^2$, with asymmetric C–O stretch at 1541 cm^{-1} or $\mu_2\text{-}\eta^3$ Class I at 1321 cm^{-1} are less likely since they are not stable at elevated temperatures [50,51].

The intensities of adsorbed CO_2 species increase for K_2O promoted catalysts, which is consistent with the CO_2 -TPD findings. For the supported 5% $\text{K}_2\text{O}/19\% \text{WO}_3/\text{Al}_2\text{O}_3$ catalyst, three IR bands are observed at 1684, 1659 and 1344 cm^{-1} (Fig. 7c). The IR band at 1684 cm^{-1} represents bidentate-I species that desorbed at 150 °C. The IR band at 1659 cm^{-1} represented bicarbonate species that desorbed at ~125 °C. The IR band at 1344 cm^{-1} disappears much faster than the higher wavenumber peaks and can be associated with monodentate species that desorbed at ~50 °C. The 2.5% $\text{K}_2\text{O}/19.5\% \text{WO}_3/\text{Al}_2\text{O}_3$ catalyst only exhibit a characteristic IR band at 1639 cm^{-1} (Fig. 7d) that starts to desorb at ~125 °C and is assigned to bicarbonate species.

The CO_2 temperature-programmed IR spectroscopy of the catalysts after the SO_2 pretreatment are presented in Fig. 8. Interestingly, the supported 20 and 21% $\text{WO}_3/\text{Al}_2\text{O}_3$ catalysts contain adsorbed species analogous to those shown in Fig. 7 after CO_2 adsorption with no obvious SO_2 species observed. This is due to the weak interactions between the SO_2 and $\text{WO}_3/\text{Al}_2\text{O}_3$ and different molar extinction coefficient for $\text{CO}_{2,\text{ads}}$ and $\text{SO}_{2,\text{ads}}$. On the $\gamma\text{-Al}_2\text{O}_3$ support, many surface species form depending on the termination of $\gamma\text{-Al}_2\text{O}_3$ and its degree of dehydration. In general, they range from weakly bound SO_2 coordinated to surface Al-OH, AlO or Al sites with vibrations at 1334, 1322, 1255–1189 cm^{-1} , respectively, while adsorbed sulfite, AlOSO_2 , exhibits a band at 1135 cm^{-1} [52,53]. The absence of these bands in Fig. 8a and b suggests limited availability of adsorption sites due to the near monolayer surface WO_x coverage.

For the supported 5% $\text{K}_2\text{O}/19\% \text{WO}_3/\text{Al}_2\text{O}_3$ catalyst, the IR bands at 1740 and 1670 cm^{-1} represent the bridged carbonate species, and the bands at 1639 cm^{-1} are assigned to bidentate-I species which desorb at 150 °C. The band at 1394 cm^{-1} is assigned to the formation of aluminum sulfate, $\text{Al}_2(\text{SO}_4)_3$ and the band at 1313 cm^{-1} is assigned to the physisorbed SO_2 species [40,52,53]. The supported 2.5% $\text{K}_2\text{O}/19.5\% \text{WO}_3/\text{Al}_2\text{O}_3$ catalyst exhibits an IR band at 1637 cm^{-1} ($T_d = 255$ °C) that is attributed to bidentate-II species. The IR band at 1390 cm^{-1} is attributed to the formation of aluminum sulfate, $\text{Al}_2(\text{SO}_4)_3$ [54]. The characteristic band at 1371 cm^{-1} represented the asymmetric stretching of the SO_2 vibration and the band at 1325 cm^{-1} is attributed to physisorbed SO_2 species [47,54,55]. The peak assignment of DRIFT spectra obtained under two different conditions are summarized in Table 2.

4. Conclusions

This work elucidates the fundamental aspects of the molecular structures and surface chemistry of supported $\text{WO}_3/\text{Al}_2\text{O}_3$ based catalysts in acidic gas CO_2 and SO_2 environments. Based on the data presented in Figs. 7 and 8, the pictorial representation of the complex interplay between the catalyst active sites and the adsorbed species is summarized in Fig. 9.

Surface WO_x species dominate un-promoted and K_2O -promoted supported $\text{WO}_3/\text{Al}_2\text{O}_3$ catalysts. For dehydrated supported $\text{WO}_3/\text{Al}_2\text{O}_3$ catalysts with high tungsten oxide coverage, the surface contain both isolated and WO_x sites. With increasing potassium oxide loading, the surface WO_x sites become more isolated. The isolated surface WO_x sites on Al_2O_3 are difficult to reduce while K_2O promotion improves reduction of surface WO_x sites at elevated temperatures. For the monolayer covered supported $\text{WO}_3/\text{Al}_2\text{O}_3$ catalysts, CO_2 adsorption results in weakly bound surface bicarbonate species and addition of K_2O changed both the surface carbonate speciation and the CO_2 adsorption capacity. The adsorption of CO_2 on the supported $\text{WO}_3/\text{Al}_2\text{O}_3$ catalyst mostly results in surface bidentate species. On the K_2O -promoted supported $\text{WO}_3/\text{Al}_2\text{O}_3$ catalyst, surface bidentate and monodentate species are mainly formed. After SO_2 pretreatment, the new sulfate stretching modes are observed over K_2O -promoted catalyst, but carbonate stretching vibrations also exist showing a competitive adsorption. With SO_2 pretreatment, the capacity of CO_2 adsorption was suppressed while supported 5% $\text{K}_2\text{O}/19\% \text{WO}_3/\text{Al}_2\text{O}_3$ catalyst showed the best resistance. As a result, the promotion of K_2O for direct synthesis of methyl mercaptan from sour gas can be attributed to 1) enhanced H_2 adsorption and/or dissociation, 2) increased CO_2 adsorption and 3) improved resistance to strong acidic condition for CO_2 adsorption.

Acknowledgements

This work is supported by the Center for Understanding and Control of Acid Gas-Induced Evolution of Materials for Energy (UNCAGE-ME), an Energy Frontier Research Center funded by U.S. Department of Energy, Office of Science, Basic Energy Sciences under grant DE-SC0012577. Part of the work including the DRIFTS and MS was conducted at the Center for Nanophase Materials Sciences, which is a DOE Office of Science User Facility. BNL Center for Functional Nanomaterials (CFN) is acknowledged for STEM studies. This research used Hitachi2700C STEM of the Center for Functional Nanomaterials, which is a U.S. DOE Office of Science Facility, at Brookhaven National Laboratory under Contract No. DE-SC0012704. Dr. Si Luo (Oak Ridge National Laboratory) is acknowledged for measuring BET surface areas.

Appendix A. Supplementary data

Supplementary material related to this article can be found, in the online version, at doi:<https://doi.org/10.1016/j.apcatb.2018.03.044>.

References

- [1] F. Lallemand, A. Rocher, N. Aimard, Sour gas production: moving from conventional to advanced environmentally friendly schemes, SPE International Heavy Oil Conference & Exhibition, Beijing, China, 2006 p. SPE 103802–SPE 103802.
- [2] O.R. Rivas, J.M. Prausnitz, Sweetening of sour natural gases by mixed-solvent absorption: Solubilities of ethane, carbon dioxide, and hydrogen sulfide in mixtures of physical and chemical solvents, *AIChE J.* 25 (1979) 975–984, <http://dx.doi.org/10.1002/aic.690250608>.
- [3] T. Chakravarty, U.K. Phukan, R.H. Weiland, Reaction of acid gases with mixture of amines, *Chem. Eng. Prog.* 81 (1985) 32–36.
- [4] L. Kucka, I. Müller, E.Y. Kenig, A. Góral, On the modelling and simulation of sour gas absorption by aqueous amine solutions, *Chem. Eng. Sci.* 58 (2003) 3571–3578, [http://dx.doi.org/10.1016/S0009-2509\(03\)00255-0](http://dx.doi.org/10.1016/S0009-2509(03)00255-0).
- [5] W. Taifan, J. Baltrusaitis, Minireview: direct catalytic conversion of sour natural gas (CH₄ + H₂S + CO₂) components to high value chemicals and fuels, *Catal. Sci. Technol.* 7 (2017) 2919–2929, <http://dx.doi.org/10.1039/C7CY00272F>.
- [6] W. Taifan, A.A. Arvidsson, E. Nelson, A. Hellman, J. Baltrusaitis, CH₄ and H₂S reforming to CH₃SH and H₂ catalyzed by metal-promoted Mo₆S₈ clusters: a first-principles micro-kinetic study, *Catal. Sci. Technol.* (2017), <http://dx.doi.org/10.1039/C7CY00857K>.
- [7] W. Taifan, J. Baltrusaitis, CH₄ conversion to value added products: potential, limitations and extensions of a single step heterogeneous catalysis, *Appl. Catal. B Environ.* 198 (2016) 525–547, <http://dx.doi.org/10.1016/j.apcatb.2016.05.081>.
- [8] P.D. Clark, N.I. Dowling, M. Huang, Conversion of CS₂ and COS over alumina and titania under Claus process conditions: reaction with H₂O and SO₂, *Appl. Catal. B Environ.* 31 (2001) 107–112, [http://dx.doi.org/10.1016/S0926-3373\(00\)00272-1](http://dx.doi.org/10.1016/S0926-3373(00)00272-1).
- [9] J. Baltrusaitis, E.V. Patterson, C. Hatch, Computational studies of CO₂ activation via photochemical reactions with reduced sulfur compounds, *J. Phys. Chem. A* 116 (2012) 9331–9339, <http://dx.doi.org/10.1021/jp3051092>.
- [10] V. Hulea, E. Huguet, C. Cammarano, A. Lacarriere, R. Durand, C. Leroi, R. Cadours, B. Coq, Conversion of methyl mercaptan and methanol to hydrocarbons over solid acid catalysts - a comparative study, *Appl. Catal. B Environ.* 144 (2014) 547–553, <http://dx.doi.org/10.1016/j.apcatb.2013.07.056>.
- [11] C. Cammarano, E. Huguet, R. Cadours, C. Leroi, B. Coq, V. Hulea, Selective transformation of methyl and ethyl mercaptans mixture to hydrocarbons and H₂S on solid acid catalysts, *Appl. Catal. B Environ.* 156–157 (2014) 128–133, <http://dx.doi.org/10.1016/j.apcatb.2014.03.026>.
- [12] E. Huguet, B. Coq, R. Durand, C. Leroi, R. Cadours, V. Hulea, A highly efficient process for transforming methyl mercaptan into hydrocarbons and H₂S on solid acid catalysts, *Appl. Catal. B Environ.* 134–135 (2013) 344–348, <http://dx.doi.org/10.1016/j.apcatb.2013.01.037>.
- [13] C. Chang, A.J. Silvestri, C.D. Chang, A.J. Silvestri, The conversion of methanol and other O-compounds to hydrocarbons over zeolite catalysts, *J. Catal.* 47 (1977) 249–259, [http://dx.doi.org/10.1016/0021-9517\(77\)90172-5](http://dx.doi.org/10.1016/0021-9517(77)90172-5).
- [14] J. Baltrusaitis, T. Bučko, W. Michaels, M. Makkee, G. Mul, Catalytic methyl mercaptan coupling to ethylene in chabazite: DFT study of the first CC bond formation, *Appl. Catal. B Environ.* 187 (2016) 195–203, <http://dx.doi.org/10.1016/j.apcatb.2016.01.021>.
- [15] N. Koivikko, T. Laitinen, S. Ojala, S. Pitkäaho, A. Kucherov, R.L. Keiski, Formaldehyde production from methanol and methyl mercaptan over titania and vanadia based catalysts, *Appl. Catal. B Environ.* 103 (2011) 72–78, <http://dx.doi.org/10.1016/j.apcatb.2011.01.010>.
- [16] S.A. Butter, A.T. Jurewicz, W.W. Kaeding, Conversion of alcohols, mercaptans, sulfides, halides and/or amines, US3894107 A, 1975.
- [17] A. Cordova, P. Blanchard, H. Salembier, C. Lancelot, G. Frémy, C. Lamontier, Direct synthesis of methyl mercaptan from H₂/CO/H₂S using tungsten based supported catalysts: Investigation of the active phase, *Catal. Today* 292 (2017) 143–153, <http://dx.doi.org/10.1016/j.cattod.2016.10.032>.
- [18] O.Y. Gutiérrez, C. Kaufmann, J.A. Lercher, Influence of potassium on the synthesis of methanethiol from carbonyl sulfide on sulfided Mo/Al₂O₃ catalyst, *ChemCatChem* 3 (2011) 1480–1490, <http://dx.doi.org/10.1002/cctc.201100124>.
- [19] A. Chen, Q. Wang, Q. Li, Y. Hao, W. Fang, Y. Yang, Direct synthesis of methanethiol from H₂S-rich syngas over sulfided Mo-based catalysts, *J. Mol. Catal. A Chem.* 283 (2008) 69–76, <http://dx.doi.org/10.1016/j.molcata.2007.12.014>.
- [20] J. Barrault, M. Boulouguiz, C. Forqy, R. Maurel, Synthesis of methyl mercaptan from carbon oxides and H₂S with tungsten–alumina catalysts, *Appl. Catal.* 33 (1987) 309–330, [http://dx.doi.org/10.1016/S0166-9834\(00\)83064-X](http://dx.doi.org/10.1016/S0166-9834(00)83064-X).
- [21] M. Taoufik, E. Le Roux, J. Thivolle-Cazat, C. Copréret, J.-M. Basset, B. Maunders, G.J. Sunley, Alumina supported tungsten hydrides, new efficient catalysts for alkane metathesis, *Top. Catal.* 40 (2006) 65–70, <http://dx.doi.org/10.1007/s11244-006-0108-4>.
- [22] S. Lwin, I.E. Wachs, Olefin metathesis by supported metal oxide catalysts, *ACS Catal.* 4 (2014) 2505–2520, <http://dx.doi.org/10.1021/cs500528h>.
- [23] R.D. Oades, S.R. Morris, R.B. Moyes, Alumina-supported tungsten catalysts for the hydrogenation of carbon monoxide, *Catal. Today* 10 (1991) 379–385, [http://dx.doi.org/10.1016/0920-5861\(91\)80019-6](http://dx.doi.org/10.1016/0920-5861(91)80019-6).
- [24] M. Maccarrone, G. Torres, C. Lederhos, J. Badano, C. Vera, M. Quiroga, J. Yori, Kinetic study of the partial hydrogenation of 1-heptyne on tungsten oxide supported on alumina, *J. Chem. Technol. Biotechnol.* 87 (2012) 1521–1528, <http://dx.doi.org/10.1002/jctb.3778>.
- [25] M. Massa, A. Andersson, E. Finocchio, G. Busca, Gas-phase dehydration of glycerol to acrolein over Al₂O₃, SiO₂-, and TiO₂-supported Nb- and W-oxide catalysts, *J. Catal.* 307 (2013) 170–184, <http://dx.doi.org/10.1016/j.jcat.2013.07.022>.
- [26] C.D. Baertsch, K.T. Komala, Y.-H. Chua, E. Iglesias, Genesis of Brønsted acid sites during dehydration of 2-butanol on tungsten oxide catalysts, *J. Catal.* 205 (2002) 44–57, <http://dx.doi.org/10.1006/jcat.2001.3426>.
- [27] T. Kabe, W.H. Qian, A. Funato, Y. Okoshi, A. Ishihara, Hydrodesulfurization and hydrogenation on alumina-supported tungsten and nickel-promoted tungsten catalysts, *Phys. Chem. Chem. Phys.* 1 (1999) 921–927, <http://dx.doi.org/10.1039/a807913g>.
- [28] H. Wang, Z. Liu, Y. Wu, Z. Yao, W. Zhao, W. Duan, K. Guo, Preparation of highly dispersed W/Al₂O₃ hydrodesulfurization catalysts via a microwave hydrothermal method: Effect of oxalic acid, *Arab. J. Chem.* 9 (2016) 18–24, <http://dx.doi.org/10.1016/j.arabjc.2014.11.023>.
- [29] R. Zhang, J. Jagiello, J.F. Hu, Z.-Q. Huang, J.A. Schwarz, A. Datye, Effect of WO₃ loading on the surface acidity of WO₃/Al₂O₃ composite oxides, *Appl. Catal. A Gen.* 84 (1992) 123–139, [http://dx.doi.org/10.1016/0926-860X\(92\)80111-O](http://dx.doi.org/10.1016/0926-860X(92)80111-O).
- [30] I.E. Wachs, T. Kim, E.J. Ross, Catalysis science of the solid acidity of model supported tungsten oxide catalysts, *Catal. Today* 116 (2006) 162–168, <http://dx.doi.org/10.1016/j.cattod.2006.02.085>.
- [31] J.A. Horsley, I.E. Wachs, J.M. Brown, G.H. Via, F.D. Hardcastle, Structure of surface tungsten oxide species in the tungsten trioxide/alumina supported oxide system from x-ray absorption near-edge spectroscopy and Raman spectroscopy, *J. Phys. Chem.* 91 (1987) 4014–4020, <http://dx.doi.org/10.1021/j100299a018>.
- [32] D.S. Kim, M. Ostromecki, I.E. Wachs, Surface structures of supported tungsten oxide catalysts under dehydrated conditions, *J. Mol. Catal. A Chem.* 106 (1996) 93–102, [http://dx.doi.org/10.1016/1381-1169\(95\)00186-7](http://dx.doi.org/10.1016/1381-1169(95)00186-7).
- [33] T. Kim, A. Burrows, C.J. Kiely, I.E. Wachs, Molecular/electronic structure-surface acidity relationships of model-supported tungsten oxide catalysts, *J. Catal.* 246 (2007) 370–381, <http://dx.doi.org/10.1016/j.jcat.2006.12.018>.
- [34] V.Y. Mashkin, V.M. Kudenko, A.V. Mashkina, Kinetics of the catalytic reaction between methanol and hydrogen sulfide, *Ind. Eng. Chem. Res.* 34 (1995) 2964–2970, <http://dx.doi.org/10.1021/ie00048a006>.
- [35] C.J. Keturakis, F. Ni, M. Spicer, M.G. Beaver, H.S. Caram, I.E. Wachs, Monitoring solid oxide CO₂ capture sorbents in action, *ChemSusChem* 7 (2014) 3459–3466, <http://dx.doi.org/10.1002/cssc.201402474>.
- [36] M.E. McBriarty, D.E. Ellis, Cation synergies affect ammonia adsorption over VOX and (V,W)Ox dispersed on α -Al₂O₃ (0001) and α -Fe₂O₃ (0001), *Surf. Sci.* 651 (2016) 41–50, <http://dx.doi.org/10.1016/j.susc.2016.03.015>.
- [37] E.I. Ross-Medgaarden, I.E. Wachs, Structural determination of bulk and surface tungsten oxides with UV-vis diffuse reflectance spectroscopy and raman spectroscopy, *J. Phys. Chem. C* 111 (2007) 15089–15099, <http://dx.doi.org/10.1021/jpc74219c>.
- [38] M.M. Ostromecki, L.J. Burcham, I.E. Wachs, N. Ramani, J.G. Ekerdt, The influence of metal oxide additives on the molecular structures of surface tungsten oxide species on alumina: I. Ambient conditions, *J. Mol. Catal. A Chem.* 132 (1998) 43–57, [http://dx.doi.org/10.1016/S1381-1169\(97\)00226-4](http://dx.doi.org/10.1016/S1381-1169(97)00226-4).
- [39] M.E. McBriarty, G.P. Campbell, T.L. Drake, J.W. Elam, P.C. Stair, D.E. Ellis, M.J. Bedzyk, Atomic-scale view of VOX-WOX coreduction on the α -Al₂O₃ (0001) surface, *J. Phys. Chem. C* 119 (2015) 16179–16187, <http://dx.doi.org/10.1021/acs.jpcc.5b04802>.
- [40] S. Soled, L.L. Murrell, I.E. Wachs, G.B. McVicker, L.G. Sherman, S. Chan, N.C. Dispenziere, R.T.K. Baker, Solid state chemistry of tungsten oxide supported on alumina, *Solid State Chem. Catal.* (1985) 165–182, <http://dx.doi.org/10.1021/bk-1985-0279.ch010>.
- [41] S.S. Enumula, V.R.B. Gurram, R.R. Chada, D.R. Burri, S.R.R. Kamaraju, Clean synthesis of alkyl levulinate from levulinic acid over one pot synthesized WO₃-SBA-16 catalyst, *J. Mol. Catal. A Chem.* 426 (2017) 30–38, <http://dx.doi.org/10.1016/j.molcata.2016.10.032>.
- [42] K.B. Ghoreishi, M.A. Yarmo, N.M. Nordin, M.W. Samsudin, Enhanced catalyst activity of WO₃ using polypyrole as support for acidic esterification of glycerol with acetic acid, *J. Chem.* 2013 (2013) 1–10, <http://dx.doi.org/10.1155/2013/264832>.
- [43] A. Ulgen, W.F. Hoelderich, Conversion of glycerol to acrolein in the presence of WO₃/TiO₂ catalysts, *Appl. Catal. A Gen.* 400 (2011) 34–38, <http://dx.doi.org/10.1016/j.apcata.2011.09.010>.

1016/j.apcata.2011.04.005.

[44] A. Chakrabarti, M.E. Ford, D. Gregory, R. Hu, C.J. Keturakis, S. Lwin, Y. Tang, Z. Yang, M. Zhu, M.A. Bañares, I.E. Wachs, A decade + of operando spectroscopy studies, *Catal. Today* 283 (2017) 27–53, <http://dx.doi.org/10.1016/j.cattod.2016.12.012>.

[45] G. Ramis, G. Busca, C. Cristiani, L. Lietti, P. Forzatti, F. Bregani, Characterization of tungsta-titania catalysts, *Langmuir* 8 (1992) 1744–1749, <http://dx.doi.org/10.1021/la00043a010>.

[46] P. Iyngaran, D.C. Madden, D.A. King, S.J. Jenkins, Infrared spectroscopy of ammonia on iron: thermal stability and the influence of potassium, *J. Phys. Chem. C* 118 (2014) 12184–12194, <http://dx.doi.org/10.1021/jp409718x>.

[47] G. Busca, V. Lorenzelli, Infrared spectroscopic identification of species arising from reactive adsorption of carbon oxides on metal oxide surfaces, *Mater. Chem.* 7 (1982) 89–126, [http://dx.doi.org/10.1016/0390-6035\(82\)90059-1](http://dx.doi.org/10.1016/0390-6035(82)90059-1).

[48] W. Taifan, J.-F. Boily, J. Baltrusaitis, Surface chemistry of carbon dioxide revisited, *Surf. Sci. Rep.* 71 (2016) 595–671, <http://dx.doi.org/10.1016/j.surfre.2016.09.001>.

[49] W.J. Schlientz, Y. Lavender, N. Welcman, R.B. King, J.K. Ruff, The chemistry of the dinuclear carbonyls anions VI. Anionic metal carbonyl carboxylates, *J. Organomet. Chem.* 33 (1971) 357–364, [http://dx.doi.org/10.1016/S0022-328X\(00\)87419-7](http://dx.doi.org/10.1016/S0022-328X(00)87419-7).

[50] D.H. Gibson, J.O. Franco, J.M. Mehta, M.S. Mashuta, J.F. Richardson, Synthesis and characterization of CO₂-bridged bimetallic compounds derived from a rhenium metallocarboxylate. Correlation of IR spectral data with coordination geometry and bonding type, *Organometallics* 14 (1995) 5068–5072, <http://dx.doi.org/10.1021/om00011a028>.

[51] D.H. Gibson, Carbon dioxide coordination chemistry: metal complexes and surface-bound species. What relationships? *Coord. Chem. Rev.* 185–186 (1999) 335–355, [http://dx.doi.org/10.1016/S0010-8545\(99\)00021-1](http://dx.doi.org/10.1016/S0010-8545(99)00021-1).

[52] A. Datta, R.G. Cavell, R.W. Tower, Z.M. George, Claus catalysis. 1. Adsorption of sulfur dioxide on the alumina catalyst studied by FTIR and EPR spectroscopy, *J. Phys. Chem.* 89 (1985) 443–449, <http://dx.doi.org/10.1021/j100249a014>.

[53] J.M.H. Lo, T. Ziegler, P.D. Clark, SO₂ adsorption and transformations on γ -Al₂O₃ surfaces: a density functional theory study, *J. Phys. Chem. C* 114 (2010) 10444–10454, <http://dx.doi.org/10.1021/jp910895g>.

[54] X.H. Lin, X.J. Yin, J.Y. Liu, S.F. Yan Li, Elucidation of structures of surface sulfate species on sulfated titania and mechanism of improved activity, *Appl. Catal. B Environ.* 203 (2017) 731–739, <http://dx.doi.org/10.1016/j.apcatb.2016.10.068>.

[55] G. Paiaro, L. Pandolfo, The organometallic chemistry of carbon suboxide, *Comments Inorg. Chem.* 12 (1991) 213–235, <http://dx.doi.org/10.1080/02603599108053475>.